NJC

# Identifying Molecular Fluorophore Impurities in the Synthesis of Low-Oxygen-Content, Carbon Nanodots Derived from Pyrene

| | |
|---|---|
| Journal: | *New Journal of Chemistry* |
| Manuscript ID | NJ-ART-01-2022-000430.R1 |
| Article Type: | Paper |
| Date Submitted by the Author: | 30-Mar-2022 |
| Complete List of Authors: | Kim, Doo Young; University of Kentucky, Department of Chemistry Kothalawala, Nadeesha Lakmali ; University of Kentucky Kim, Sang Won; Samsung Advanced Institute of Technology, Inorganic Materials Lab Kim, Namhee; Yonsei University College of Science, Chemistry Henderson, Collan; University of Kentucky, Chemistry Seol, Minsu; Samsung Advanced Institute of Technology, Yang, Fuqian; University of Kentucky, Chemical and Materials Engineering Kwak, SeungYoun; Samsung Advanced Institute of Technology Hwang, Kyu Young; Samsung Advanced Institute of Technology SON, WON-JOON; Samsung Advanced Institute of Technology, Shin, Hyeon-Jin; Samsung Advanced Institute of Technology Choi, Hyeonho; Samsung Electronics, Samsung Advanced Institute of Technology Kim, Byeong-Su; Yonsei University, Department of Chemistry |
| | |

SCHOLARONE™
Manuscripts

# Identifying Molecular Fluorophore Impurities in the Synthesis of Low-Oxygen-Content, Carbon Nanodots Derived from Pyrene

Nadeesha L. Kothalawala,[a†] Sang Won Kim,[b†] Nam Hee Kim,[c†] Collan J. Henderson,[a] Minsu Seol,[b] Fuqian Yang,[d] Seung-Yeon Kwak,[b] Kyu Young Hwang,[b] Won-Joon Son,[b] Hyeon-Jin Shin,*[b] Hyeonho Choi,*[b] Byeong-Su Kim*[b], Doo Young Kim*[a]

Carbon dots (C-dots) are a promising class of carbonaceous nanomaterials for bioimaging, catalysis, and optoelectronics. However, their applications are alarmed by recent reports that bright molecular fluorophores are co-produced in the synthesis of C-dots, in particular ones prepared through bottom-up approach (carbon nanodots (CND)), commonly derived from citric acid precursor. The presence of highly emissive molecular fluorophore species obscures true performance of CND and severely challenges the development of CND. Here we observe that the issue of molecular fluorophore impurity is still problematic for CND which are derived from a different type of precursor, polycylic aromatic hydrocarbons (PAHs).  In this study, low-oxygen-content CND and small molecular fluorophores are co-produced through hydrothermal condensation of nitropyrene. Extensive and systematic characterizations following column chromatographic separation and solvent-induced extraction reveal that molecular fluorophores and CND are clearly dissimilar in structure and optical properties. This work highlights that rigorous separation and purification steps need to be taken for not only hydrophilic CND but also low-oxygen-content CND.

## Introduction

Carbon dots (C-dots) are a promising class of carbonaceous nanomaterials with attractive properties such as tunable photoluminescence, catalytic activity, photostability, and low cytotoxicity.[1-3] Low cost of synthesis and abundance of source materials are significant merits of C-dots.[4] Due to these appealing features, C-dots are considered well-suited to optoelectronics,[5, 6] energy conversion and storage,[7-9] and biomedical applications.[3, 10-12] C-dots are typically synthesized through two methods, top-down synthesis and bottom-up synthesis. In the top-down synthesis, bulk graphitized carbon materials (carbon black, carbon fiber, graphene oxide, or graphene) are cut into nano-sized particles through acidic oxidation, solvothermal methods, microwave, and sonication assisted method.[13, 14] Bottom-up synthesis involves the assembly of nanoscale carbonaceous particles built from small precursor molecules. Throughout this work, C-dots specifically produced through bottom-up approach will be labeled as carbon nanodots (CND) [15] to distinguish them from ones

synthesized by top-down method. A variety of source materials were utilized  for the production of CND including citric acid, glucose, and polycyclic aromatic hydrocarbon.[16] Since the initial discoveries of tunable photoluminescence (PL), development of CND for light emitting diodes has been actively pursued, [17-19]with the basic strategy of tuning PL properties by either controlling the size and shape of the particles (diameter of delocalized graphitic core) or creating functional groups on their periphery.[20-28]

In spite of noticeable progress made in the field, the development of C-dots was severely alarmed by recent reports that the synthesis of C-dots, in particular of CND through bottom-up methods, likely involve the co-production of brightly emissive molecular fluorophores.[29, 30] For example, fluorescent molecular species were formed during hydrothermal synthesis from citric acid.[31-33] Yang et al. have isolated molecular fluorophores using silica column chromatography and identified them as an incomplete condensation product generated during hydrothermal synthesis with citric acid and diethylamine precursors.[32] Shi et al. have reported the formation of small organic molecular fluorophores during bottom-up synthesis using citric acid and L-cysteine.[33] In these reports, co-produced molecular fluorophore species were distinctive from CND in size, structure, morphology, and optical properties.

Unfortunately, little attention has been paid to this issue of molecular fluorophore impurity generated in the synthesis of CND until recently, often leading to the misleading interpretation of CND properties. Because of this issue, the origin of bright and tunable PL from CND is still disputable. The presence of molecular emitter impurities hinders the further

a. Department of Chemistry, University of Kentucky, Lexington, Kentucky, 40506, USA.
b. Samsung Advanced Institute of Technology (SAIT), Samsung Electronics Co. Ltd., Suwon 16678, Republic of Korea.
c. Department of Chemistry, Yonsei University, 50 Yonsei-ro, Seoul 03722, Republic of Korea.
d. Materials Program, Department of Chemical and Materials Engineering, University of Kentucky, Lexington, KY 40506, USA.
†These authors contributed equally to this work.

advance of CND. The separation of molecular fluorophore impurities is of utmost importance to identify the source of PL in CND. It is generally straightforward to separate molecular fluorophores from CND by column chromatography and dialysis,[30] but the separation may be complicated when two parts are linked through covalent bond.[30] Although several articles reported the formation of molecular fluorophores, investigations were limited to the production of CND with citric acid precursor. This problem was not investigated for other types of precursors, for example, polycyclic aromatic hydrocarbon (PAH) compounds. While CND from citric acid, most common type of precursor molecule, are typically rich of oxygen (30% - 45% oxygen content) and highly disordered in structure,[34, 35] CND from PAHs are more ordered with less content of oxygen.[28, 36]

Herein we report the synthesis of CND through the condensation of substituted PAH, 1,3,6-trinitropyrene (TNP). Molecular fluorophores were separated from CND by silica column chromatography. The composition and optical properties of each fraction were thoroughly analyzed to identify molecular fluorophore and CND. Molecular fluorophores exhibited much brighter emissions than CND. The separation of molecular fluorophores and CND was also accomplished by solvent washout. Dissimilar physicochemical properties, morphologies, chemical structures, and optical properties of molecular fluorophore and CND were confirmed by dialysis in methanol, PL measurements, thermogravimetric analysis (TGA),

separation of bright emitting molecular fluorophores from low emitting CND through diverse extraction methods.

## Experimental

### Materials

All chemicals and solvents used for the syntheses were purchased from commercial suppliers and used without further purification. Pyrene (99%), HNO$_3$ (70%), NaOH (99%), and HCl (35~37%) were purchased from Sigma-Aldrich. PVDF membrane filters were purchased from Merck Millipore.

### Synthesis of CND

2 gram of pyrene was nitrated in HNO$_3$ (70%, 160 mL) at 80 °C for 12 hours to produce 1,3,6-trinitropyrene (TNP).[28] After cooling to room temperature, the mixture was filtered and neutralized with NaOH. The resultant powder of TNP (6 gram) was dispersed in NaOH (0.2M, 1L) solution under ultrasonication for 1 hour. The suspension was transferred into an autoclave, then heated at 300 °C for 10 hours. The product was filtered with PVDF membrane filter (pore size 200 nm) to remove insoluble carbon product and HCl (70%) was added to the filtered solution dropwise. When the medium is made acidic the solubility of CND is decreased due to the protonation of acidic functional groups such as carboxylic and phenolic groups. Hence, CND start to aggregate and precipitate in the solution which enable separation of the CND through centrifugation. The



Scheme 1. Procedures to synthesize CNDs and separate fractions through column chromatography. At the bottom, it presents the hypothetic scheme of the synthesis starting from pyrene, to TNP, and to CND.

X-ray photoelectron spectroscopy (XPS), Fourier transform Infra-red spectroscopy (FT-IR), Raman spectroscopy, matrix-assisted laser desorption/ionization time-of-flight (MALDI-TOF) mass spectrometry, transmission electron microscopy (TEM), and X-ray diffraction analysis (XRD). We identified the molecular fluorophores as incomplete condensation products of TNP. The results reported in this work manifests the systematic

product was separated from the liquid using a centrifuge at 15000 rpm for 10 minutes. The obtained CND were dried at 75℃ under vacuum overnight.

### Column chromatography

The as-obtained CND were separated through a Biotage Isolera flash purification system with a column bridge (IntertecTM, size of 60 g). The column cartridge was uniformly packed with silica gel as stationary phase and equilibrated with 2.5 column

volumes of solvent with low polarity. Then, the screw-top cap of the column cartridge was detached and the remaining solvent on silica gel was eliminated. Next, 0.10 g of crude CND sample was loaded on silica gel was prudently added on to the frit inside the column cartridge. The screw-top cap was then re-attached and eluted with a gradient of solvent mixture using dichloromethane (DCM) and methanol (MeOH) using normal phase column chromatography. The percentage of MeOH in the solvent mixture was changed from 0 % to 10 % (v:v) during the separation.

**Dialysis of Column Fractions**

Dialysis was carried out for each column fraction in MeOH using a regenerated cellulose dialysis membrane (1kDa MWCO) for 24 hours. The dialysate (solution outside a dialysis bag) and the retentate (solution inside a dialysis bag) were separately collected to test the photoluminescence.

**Characterizations**

UV-Vis absorbance measurements of the column fractions in MeOH were carried out using Thermo-Scientific Evolution 201 UV-Visible Spectrophotometer. The samples were scanned in the wavelength range 200 nm – 1000 nm with a bandwidth of 1 nm and 0.1 s integration time. Steady-state emission spectra of the column fractions were recorded using the Horiba Scientific Fluoromax Plus-C fluorometer. The measurements were performed at a series of excitation wavelengths using 2 nm entrance and exit slits with an integration time of 0.1 s. Fluorescence lifetime measurements were carried out using the time-correlated single-photon counting method. A DeltaHub$^{TM}$ high throughput time-correlated single-photon-counting (TCSPC) controller connected to the Horiba Scientific Fluoromax Plus-C fluorometer was used with a Nano LED as the pulsed excitation source. (Excitation wavelength 455±10 nm). The lifetimes were recorded at 584 nm, 515 nm, and 532 nm emission wavelengths, 200 ns measurement range, 5 nm bandpass, and a 1 MHz repetition rate. The instrument response factor (IRF) was obtained using Ludox solution. The lifetime decays were fit, and the lifetime calculations were carried out using Decay Analysis (DAS6) software. The decays were fit using single, two and three exponentials to calculate the lifetime. Absolute photoluminescence Quantum Yield (PLQY) measurements were performed using the integrated sphere connected to the Horiba Scientific Fluoromax Plus-C fluorometer. The excitation wavelength 480 nm. 0.5 nm slit width and 0.5 s integration time were the parameters for the PLQY measurements and the calculation of the PLQY was performed using the Horiba Scientific FluorEssence$^{TM}$ software. The spectral range was set to cover both the Rayleigh scattering peak of the excitation and the emission peak from the sample. Methanol was used as the blank and the measurement of the blank was carried out under the same condition and parameters as the sample. Calculation of PLQY was carried out based on the following equation, PLQY =$[ (P_B-P_A)/(L_A-L_B)] \times 100$ %. $P_A$ and $P_B$ are the integrated emission intensities of the blank and the sample, respectively. $L_A$ and $L_B$ are the integrated Rayleigh scattering intensities of the blank and the sample, respectively, in the range of excitation.

XPS measurements were carried out using a Thermo Scientific K-alpha X-ray photoelectron spectrometer with a monochromatic Al Kα X-ray source. The analyzed spot size was 400 μm in diameter. Measurements were carried out with the flood gun. Sample preparation was carried out by drop-casting the samples on to a thoroughly cleaned Si wafer. All the survey spectra and the high-resolution spectra were collected with 10 scans. The XPS data analysis was done by deconvoluting the spectra using Thermo Avantage software. Fourier-Transform Infrared Spectroscopy (FT-IR) measurements were conducted using a Nicolet IS50 FT-IR spectrometer with a diamond attenuated total reflectance (ATR) plate. FT-IR spectra were recorded with 4 cm$^{-1}$ resolution and 64 scans. Samples were drop-cast onto the ATR plate and then dried until the solvent evaporates inside a 60℃ oven.

MALDI-TOF mass spectra were recorded on a Bruker UltrafleXtreme spectrometer using 7,7,8,8-tetracyanoquinodimethane (TCNQ) as the matrix. XRD patterns were obtained with a Bruker D8 Discover system using Cu Kα radiation.

TGA was performed with a Q50 (TA instruments) by ramping up the temperature from 30 $^0$C to 800 $^0$C at the rate of 100C min$^{-1}$ under the flow of N$_2$ gas. TEM images in bright-field mode were collected using a JEM-F200 transmission electron microscope (JEOL). Sample preparation for TEM was conducted by drop casting the sample dispersed in dimethylformamide (DMF) on to a carefully cleaned Si wafer.

Raman spectra of column fractions were obtained using Thermo Scientific DXR micro-Raman spectrometer equipped with a diode-pump Nd:YVO$_4$ laser. Measurements were carried out at 532 nm excitation and 0.8 mW laser power. The concentrated solutions of F$_Y$, F$_G$, and F$_{CND}$ samples were mounted on a thoroughly cleaned Si wafer and dried in an oven (60$^0$C) to completely remove the solvent. Raman measurements of crude sample, pyrene and TNP were also performed for comparison.

## Results and discussion

The synthetic procedure of pyrene-derived CND is summarized in Scheme 1. This scheme also depicts a hypothetical process in which pyrene precursor is first nitrated into TNP and then fused into CND through hydrothermal condensation. TNP enhances its reactivity for hydrothermal condensation.[28, 37, 38] We observed that the fusion of TNP has led to the formation of well-ordered CND with a good crystallinity (as revealed in the TEM images in the later section), whereas conventional bottom-up pyrolysis of citric acid typically produced highly disordered CND.[39, 40] Filtration and centrifugation were performed to separate the crude CND from unreacted species. Then, column chromatography was performed to separate molecular impurities and CND. Several fractions were eluted through a silica column. Among those, three fractions (labeled as F$_Y$, F$_G$, and F$_{CND}$) showing distinctive PL behaviors were further analyzed (Figure 1).

Fig. 1(a) shows chromatographic separation of the crude sample under the illumination of UV-light (λ = 365 nm). Among F$_Y$, F$_G$, and F$_{CND}$ fractions, F$_Y$ has the shortest retention time, and it is
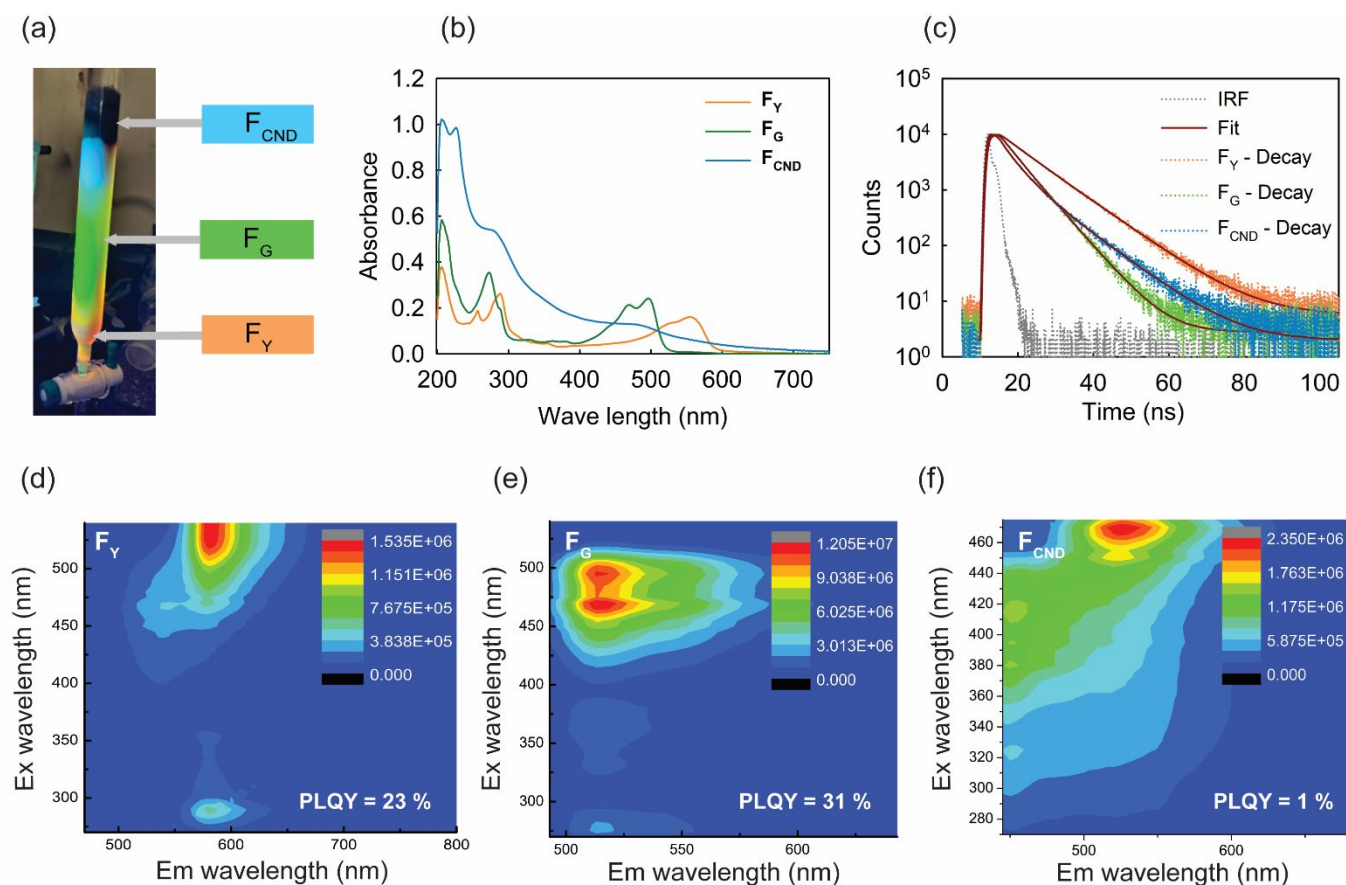
Figure 1. (a) a photograph of a silica column with the elution of three fractions, $F_Y$, $F_G$, and $F_{CND}$. (b) UV-Vis absorbance spectra of $F_Y$, $F_G$, and $F_{CND}$. (c) PL lifetime decay profiles of $F_Y$ ($\lambda_{Ex}$ = 455 nm, $\lambda_{Em}$ = 584 nm) $F_G$ ($\lambda_{Ex}$ = 455 nm, $\lambda_{Em}$ = 515 nm) and $F_{CND}$ ($\lambda_{Ex}$ = 455 nm, $\lambda_{Em}$ = 532 nm) from time correlated single photon counting (TCSPC) experiments. 3-D PL mapping spectra of (d) $F_Y$, (e) $F_G$, and (f) $F_{CND}$ (colored bars in the insets show the PL counts per second).

followed by $F_G$ and $F_{CND}$. The short retention time of $F_Y$ is attributable to its less polarizable character. As shown in the XPS data in Figure 2(a-b), $F_Y$ contains less $sp^2$-bonded carbon than $F_G$. A negatively charged, silica stationary phase of the column can polarize π electrons delocalized in the $sp^2$-bonded carbon structure, inducing molecular interaction with the stationary phase. The molecular interaction of π electrons with the stationary phase is weaker for $F_Y$ than for $F_G$, leading to the faster elution of $F_Y$. The longest retention time of $F_{CND}$ among 3 fractions is attributable to the fact that $F_{CND}$ is significantly larger than $F_Y$ and $F_G$ and has the longest π conjugation through its fully graphitized core. $F_Y$ has yellow emission at 365 nm excitation and $F_G$ gives green emission. $F_{CND}$ appears in the form of a black residue with a bluish-green emission.

UV-VIS spectra of 3 fractions ($F_Y$, $F_G$, $F_{CND}$) are shown in Fig. 1(b). The spectrum of $F_{CND}$ is noticeably different from those of $F_Y$ and $F_G$. $F_{CND}$ exhibits a very broad absorption spectrum in the range from 200 nm to 700 nm with a shoulder at 280 nm due to π-π* transitions from $sp^2$-carbon domain. A broad absorption in 400-700 nm range represents the transition of surface states present in $F_{CND}$.[28] This feature of CND is commonly reported in literature.[22] In contrast, $F_Y$ and $F_G$ present relatively sharp bands and vibronic features which are characteristic of molecular fluorophores.[30] The absorption band of $F_Y$ is shifted toward

**ARTICLE**

longer wavelength compared to $F_G$. This red shift may be due to the structural difference of two molecular species.

green emission with a peak maximum at 515 nm and $F_Y$ shows yellow emission with a peak maximum at 584 nm. The raw
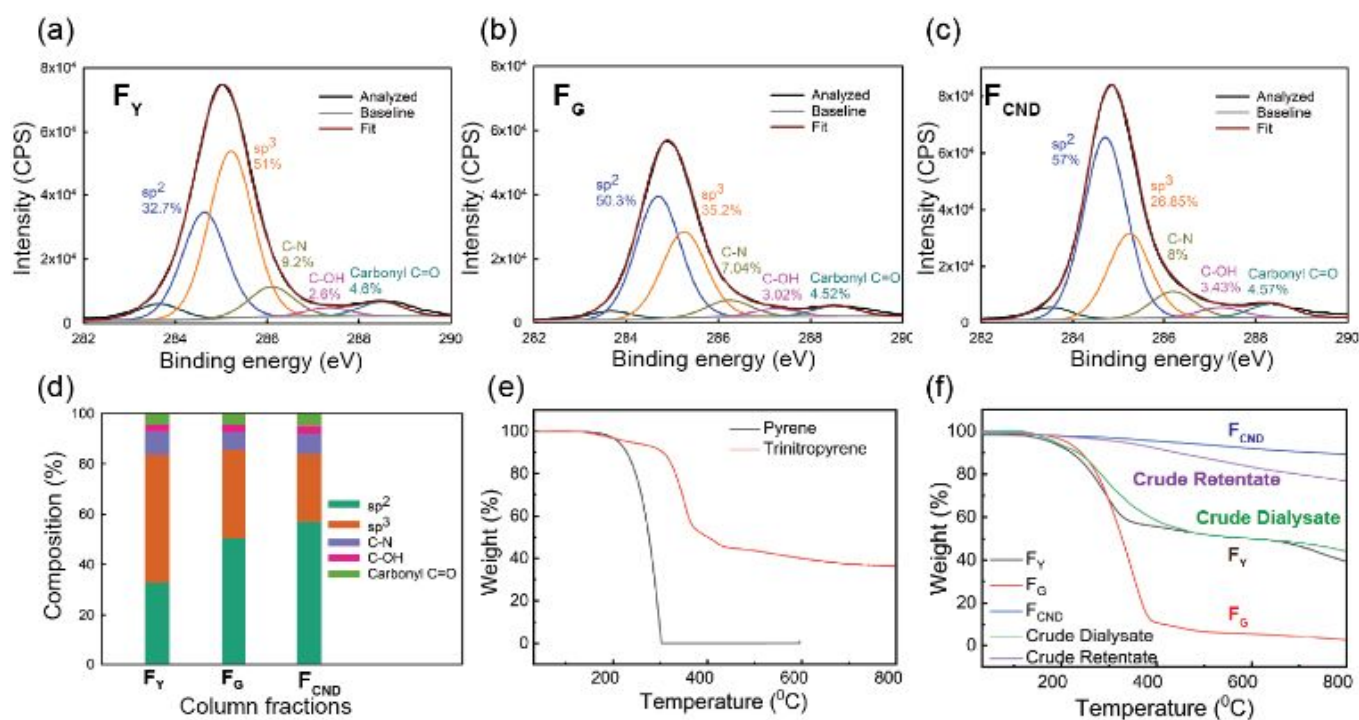


Figure 2. Deconvoluted high-resolution C1s XPS spectra of fractions (a) $F_Y$, (b) $F_G$, and (c) $F_{CND}$. (d) percentages of chemical states of carbon element in each fraction determined by XPS analysis, TGA curves of the precursors (e) TNP and pyrene, and (f) $F_Y$, $F_G$, $F_{CND}$, and crude retentate and crude dialysate from dialysis of crude sample.

Figure 1(c) presents time-resolved PL decays of $F_Y$, $F_G$ and $F_{CND}$ recorded by TCSPC experiments. TCSPC decay parameters for the three fractions are summarized in Table S1. PL decay of $F_Y$ fits well with single exponential decay at 455 nm excitation ($\tau$ = 8.9 ns). The 8.9 ns decay is much longer than the intrinsic decay component of CND which has been reported in literature, confirming that $F_Y$ emission is from molecular fluorophore.[23] $F_G$ shows bi-exponential decay with a fast decay component $\tau_1$ (3.2 ns) and slower decay component $\tau_2$ (5.7 ns). The fast $\tau_1$ component may be from an aggregated form of the molecular fluorophore. In contrast to $F_Y$ and $F_G$, the decay of $F_{CND}$ fits with three exponentials, representing complex and inhomogeneous nature of $F_{CND}$. Three decay components include a fast decay, $\tau_1$, which corresponds to intrinsic emission from $sp^2$-bonded graphitic carbon core of CND and slower decays, $\tau_2$ and $\tau_3$. $\tau_2$ and $\tau_3$ components are assigned to functional groups on the periphery of CND.[22, 30] Notably, the 3 decay components of $F_{CND}$ are in a good agreement with the PL decay of CND reported in literature which have been synthesized through a top-down method as well as a bottom-up method.[22, 23] Based on UV-VIS spectroscopy and TCSPC results, $F_Y$ and $F_G$ can be unarguably assigned to molecular fluorophores and $F_{CND}$ primarily contains CND having a larger graphitic core.

Figure 1(d-f) show 3D PL mapping of three fractions. The PL spectra of $F_G$ and $F_Y$ indicate an excitation-independent behavior, indicating the presence of one or only few chromophores in $F_G$ and $F_Y$. Conversely, the PL mapping of $F_{CND}$ shows an excitation-dependent behavior: the red-shift of emission as the excitation wavelength get longer. $F_G$ displays

emission spectra of three fractions are given in Figure S1 (d-f). The excitation-independent PL of $F_Y$ and $F_G$ along with their higher quantum yields (23 % for $F_Y$ and 31 % for $F_G$) is another piece of evidence that $F_G$ and $F_Y$ are molecular fluorophores[30, 34] formed during hydrothermal condensation of nitrated pyrene precursors. It is noteworthy that, however, UV-VIS and PL spectra of $F_Y$ and $Y_G$ are distinguishable from those of pyrene and TNP shown in Figure S1 (a-c). The excitation-dependent PL of $F_{CND}$ suggests that this fraction contains multi-chromophoric units and has a heterogeneous structure, in a good agreement with the behavior of CND commonly reported in the literature. PL quantum yield of $F_{CND}$ is very low (1%) since the main emitting species in $F_{CND}$ is weakly-emitting CND with large crystalline, graphitic core and low surface oxidation.[30] Photoluminescence excitation (PLE) spectra of $F_Y$, $F_G$, and $F_{CND}$ are presented in Figure S2. PLE spectra of $F_G$ recorded at two emissions (537 nm, 584 nm) are nearly overlapped, indicating the two emissions come from the same origin. The PLE spectra of $F_Y$ show two bands implying that two emitting species are present. The two emitting species may be ascribed to different types of molecular fluorophores with slight structural and compositional changes. The PLE spectra of $F_{CND}$ recorded at the two main emission wavelengths (455 nm and 540 nm) reveals the possibility of the presence of two emissive species. Based on the TCSPC result of $F_{CND}$ with 3 decay components, $F_{CND}$ may contain molecular fluorophores (or similar structure) covalently bonded to CND in addition to the weakly-emitting graphitic core.[30]

Figure 2(a-c) present the high resolution XPS C1s spectra of $F_Y$, $F_G$ and $F_{CND}$. The C1s high-resolution XPS spectra are

deconvoluted with peaks assigned to $sp^2$-C (284.6 eV), $sp^3$-C (285.2 eV), C-N (286.1 eV), hydroxyl C-OH (287.34 eV), and carbonyl C=O (288.5 eV). Bar graphs in Figure 2(d) summarize the percentages of various chemical states of carbon element in $F_Y$, $F_G$, and $F_{CND}$. Compared to $F_G$, $F_Y$ possesses a lower $sp^2$-C content and a higher $sp^3$-C content, indicating more abundant functional groups. $F_{CND}$ has the highest $sp^2$-C content and the least $sp^3$-C content indicating the predominant graphitic domain. In addition to the size of particles in each fraction, their content of $sp^2$-C may be an important factor to influence the retention behavior as discussed in Figure 1. Unlike CND derived from precursors of citric acid, urea, ethylenediamine, cysteine, and saccharides contain high oxygen contents, we report that PAH-derived CND contain much lower oxygen content ( <20 %, Figure S4) and a high C/O ratio.

Figure S3 presents FT-IR spectra of $F_Y$, $F_G$, $F_{CND}$, and precursor molecules. FT-IR spectra of $F_Y$ and $F_G$ display sharp peaks in the 700 – 1600 $cm^{-1}$ range corresponding to C-N stretch, $sp^3$ C-H bending, and aromatic ring stretch. TNP shows overlapping peaks in the 700 – 1600 $cm^{-1}$ indicating their structural similarity. In addition, $F_Y$ and $F_G$ present the peaks for hydroxyl groups (3400 $cm^{-1}$), amine groups (3250 – 3300 $cm^{-1}$), and carbonyl groups (1745 $cm^{-1}$). An aromatic ring stretch (1580 $cm^{-1}$) is intensified more in FY and FG than in TNP (Fig. S3(e)), indicating aromatic ring of the precursor molecule becomes extended during condensation. $F_{CND}$ also display similar functional groups and the content of $sp^3$-C but presents a marked intensity of aromatic domains (1580 $cm^{-1}$). Overall, FT-IR results are consistent with XPS data, giving a convincing conclusion that $F_{CND}$ is dominated by large $sp^2$-C graphitic domains whereas $F_G$ and $F_Y$ comprise more confined aromatic domains and functional groups.

TGA provides useful insights about the chemical structure of materials. In Figure 2(e-f), temperature driven mass loss of materials was recorded for precursor molecules (pyrene and TNP) and three fractions. All TGA experiments were carried out under the $N_2$ flow.[41] $F_Y$ loses 40 % weight around 300 ℃ and stays stable until it is decomposed at 700 ℃. This stability of $F_Y$ after 300 ℃ could be due to the rearrangement of this molecule into a stable structure in the solid form. FG has shown an extensive mass loss (90 % loss) at 400 ℃. TNP (figure 2(e)) shows 50 % weight loss at 350 ℃ indicating that $F_Y$ and TNP may contain similar structure. Pyrene resembles $F_G$ although it is

decomposed more rapidly. Unlike other samples, $F_{CND}$ shows negligible mass loss (<10% loss) until 800 ℃.[42] Presumably, large graphitized $sp^2$ carbon core in $F_{CND}$ makes it very stable against thermal decomposition. TGA analysis was also performed for the dialysate and the retentate of the crude sample (crude sample without any chromatographic separation) as shown in Figure 2(f). The dialysis of the crude sample was carried out using a 1000 Da molecular weight cut-off (MWCO) membrane for 48 hours. TGA curve of the dialysate overlaps that of $F_Y$ confirming the presence of the same molecular fluorophores in the crude dialysate. TGA curve of the retentate shows a trajectory similar to that of $F_{CND}$ indicating that CND are the predominant species retained during dialysis. Overall, TGA results provide strong evidence that small molecular fluorophores were co-produced in the synthesis of CND.

Raman spectroscopy is a sensitive tool to probe the microstructure of materials. For example, D band (1360 $cm^{-1}$) and G band (1580 $cm^{-1}$) in Raman spectrum are the signature of six-membered, graphitic carbon domains present in the sample. Figure 3 shows the Raman spectrum of $F_{CND}$ in comparison with those of $F_G$, $F_Y$, crude sample, and the precursor molecules. Some of samples produce noisy spectra due to low laser power used in acquiring the signal. This was done to avoid an adverse effect of Raman excitation laser causing structural damages and pyrolysis through heat accumulation along the surface of less conductive samples. Both D band and G band are clearly found in $F_{CND}$. $F_G$ and $F_Y$ show distinct Raman peaks different from each other and $F_{CND}$. Importantly, D and G bands are absent in $F_Y$ and $F_G$ suggesting their identity as non-graphitic molecular fluorophores. Some peaks in the spectra of $F_Y$ and $F_G$ closely overlap with those in the spectra of pyrene and TNP (Figure 3(e-f)), implying that molecular fluorophores and precursors share similar structural units. This interpretation is consistent with outcomes of TGA results. In the crude sample, D and G bands are present suggesting the presence of CND in the non-purified crude product. Figure S5 shows the TEM images of $F_Y$, $F_G$, and $F_{CND}$, respectively. While TEM images of $F_Y$ and $F_G$ show the sparse dark spots in the entire region of the sample, TEM image of $F_{CND}$ displays the dense dark dots with lateral size of approximately 3-5 nm. Figure S5(d-e) clearly show graphitic lattice fringes of particles. The spacing of 0.2 nm in the lattice fringes (Figure S5(e)) is assigned to (100) plane of graphite. Taken together, these images provide additional evidence that $F_{CND}$ is primarily composed of graphitic $sp^2$-bonded carbons unlike $F_Y$ and $F_G$.

Recent studies urged researchers to perform dialysis as a critical step to separate CND from impurities and synthesis residues. The separation of species through dialysis is based on the difference in size and solvation radii.[28, 33, 43] It was reported that small molecular fluorophores were successfully separated from CND by dialysis, and a retentate (solution inside a dialysis bag) and a dialysate (solution outside a dialysis bag) were identified as CND and molecular fluorophores, respectively.[29, 30] It is noteworthy that in most CND dialysis, water was employed as solvent because CND and co-products derived from citric acid were hydrophilic. On the contrary, our synthesis using
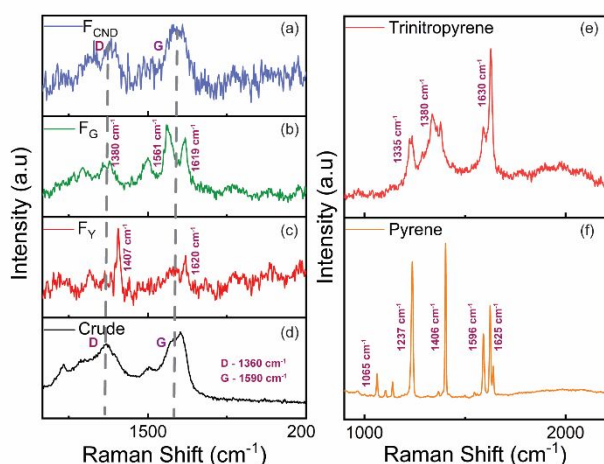


Figure 3. Raman spectra of (a) $F_{CND}$, (b) $F_G$, (c) $F_Y$, and (d) crude sample. Raman spectra of (e) TNP and (f) pyrene.

substituted polyaromatic precursor has produced hydrophobic particles, which are only sparingly soluble in water. The choice of a correct solvent is important to avoid the aggregation of materials which may interrupt size-driven permeation process across dialysis membrane. In the current study, the dialysis was carried out for 24 hours in MeOH as the fractions were dissolved in MeOH reasonably well.

The dialysis was performed with $F_{CND}$, $F_Y$ and $F_G$, three fractions which were isolated by column chromatography. Figure 4(a) illustrates the dialysis procedure and Figure 4(b-g) are the PL spectra of each fraction measured for the retentate part in comparison with the dialysate part. Note that instrument conditions for the PL experiments (e.g., slit widths, collection time) were kept same for both retentate and dialysate
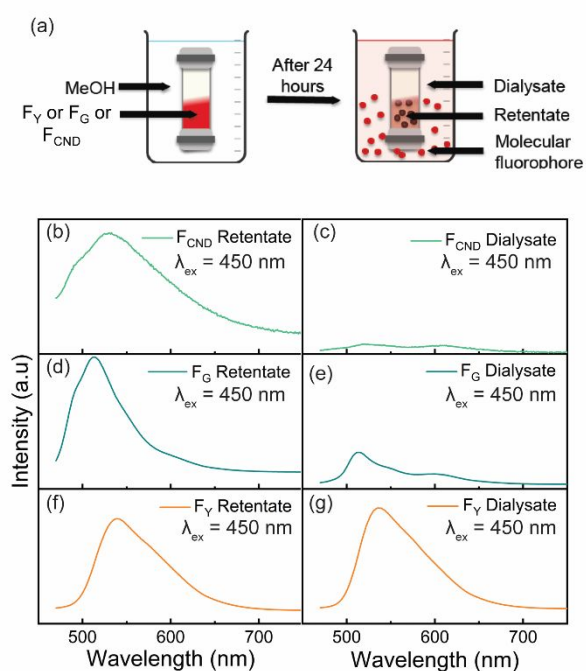


Figure 4 A schematic illustration of a dialysis procedure. PL spectra of (b) the retentate and (c) the dialysate of $F_Y$. PL spectra of (d) the retentate and (e) the dialysate of $F_G$. PL spectra of (f) the retentate and (g) the dialysate of $F_{CND}$. Note that the PLs of dialysates and retentates were immediately measured after dialysis without concentrating or diluting, and the volume ratio of the dialysate and the retentate in all the fractions is approximately 70:1.

solutions, and the solution volume of dialysate is 70 times larger than that of retentate. For $F_{CND}$, only a negligible PL intensity was observed in the dialysate (Figure 4(c)) after 24 hours of dialysis indicating very small fraction of $F_{CND}$ leaked through a dialysis bag. On the contrary, the majority of $F_Y$ and $F_G$ escaped to the dialysate. Based on the volume difference (70:1, dialysate : retentate) and the calculation of areas under PL spectra, 90 % of $F_G$ and 99 % of $F_Y$ are estimated to leak into the dialysate. Overall, our dialysis results support that $F_{CND}$ particles are significantly larger than $F_G$ and $F_Y$.

Although column chromatography and dialysis successfully separated molecular fluorophores and CND, these methods are not applicable for large-quantity samples. Therefore, a simple

solvent-based process was tested as a tool, potentially suited to a large-scale production. Acetone and aqueous ammonia solution were used as solvents to extract molecular fluorophores and CND, respectively. As shown in Figure 5, an organic solvent such as acetone is effective in extracting hydrophobic molecular fluorophores. And aqueous ammonia solution (pH 11.2) promotes the dissolution of CND by deprotonating hydroxylic groups on the periphery of CND. The detailed procedure of the solvent washouts is illustrated in Figure S6(a). After extraction with acetone and aqueous ammonia, each washout has passed through vacuum filtration to remove insoluble large particles. Acetone washout solution is denoted as $S_A$ and base washout with aqueous ammonia (pH 11.2) is denoted as $S_N$. The photographs of $S_A$ and $S_N$ are shown in Figure S6(b). It was attempted to disperse the crude sample in aqueous solution at various pH, and only pH 10.6 and 11.2 solutions successfully dispersed the crude sample (Figure S6(c)) indicating the effect of hydroxylic groups in the sample.

XRD spectra in Figure 6(a) clearly present the structural difference between $S_A$ and $S_N$. $S_N$ shows a single, broad peak at $26^o$ which is characteristic of the (002) plane of graphite, implying that graphitic carbon material is the major constituent of this sample. Although the XRD spectrum of $S_A$ also reveals the similar peak around $26^o$, it presents two additional distinct peaks at $12.1^o$ and $24^o$ that are assigned to the (001) plane and the (002) plane of pyrene derivatives, respectively. These two peaks suggest that $S_A$ contains molecular fluorophores derived from pyrene and TNP. TEM images of $S_A$ and $S_N$ are shown in Figure 5(b-c). In the case of $S_A$, we didn't observe any atomic symmetry and lattice structure. Instead, needle-like morphology with the length of 100 nm is observed (Figure 5(b), inset). This needle-like structure was similar to that of pyrene-derivatives reported in the previous publication[44] and may originate from the supramolecular assembly of molecular fluorophores. In contrast, dark circular dots with uniform lateral sizes appear in $S_N$ (Figure 5(c)) and the high-resolution TEM image of $S_N$ (Figure 5(c), inset) shows a crystalline structure with a lattice spacing of 0.21 nm corresponding to graphene (100) planes.

To obtain an insight about chemical structure of $S_A$ and $S_N$, MALDI-TOF analysis was performed. The resultant mass spectra in Figure 5(d) show very different distributions of mass-over-charge (m/z) for $S_A$ and $S_N$. While $S_N$ shows a broad m/z distribution in the 1000 − 5000 Da range with the maximal intensity around 1500 Da, $S_A$ exhibits much lower m/z centered around 700 Da. This suggests that particles in $S_A$ are quite smaller than in $S_N$. The representative MALDI-TOF signals are depicted in the insets. For $S_N$, a regular fragmentation pattern with the repeated m/z of 24 is found in the mass spectra, which is interpreted as C=C bonds of polycyclic aromatic carbon compounds.[45, 46] For $S_A$, there is no apparent fragmentation pattern in the whole m/z range. This probably means that the chemical structure of $S_A$ includes not only aromatic units but also aliphatic chains.

FT-IR analysis was performed for $S_A$ and $S_N$ to track their functional groups. In FT-IR spectra (Figure 5(e)), both samples show overlapping characteristic peaks related to the –OH

stretching vibration at 3000-3500 cm$^{-1}$, C=O stretching at 1690 cm$^{-1}$, aromatic C=C stretching at 1620 and 1570 cm$^{-1}$, C-O stretching at 1270 and 1180 cm$^{-1}$, aromatic C=C bending at 840 cm$^{-1}$, and C-H bending at 770 cm$^{-1}$. Although two samples show the similar types of functional groups, the relative intensities of peaks are somewhat different. The aromatic C=C stretching and bending peaks are stronger in $S_N$ than $S_A$, while the peaks of oxygen-containing groups are more intensified in $S_A$. These results demonstrate that $S_N$ has the chemical structure of graphitic CND, while the main component of $S_A$ is not the same as $S_N$.

## Conclusions

This work demonstrates that highly emissive molecular fluorophores are simultaneously produced in the synthesis of CND through hydrothermal condensation of substituted PAHs. By employing both column chromatography and a simple solvent-driven extraction, molecular fluorophores were successfully separated from CND. Through extensive characterizations, molecular fluorophores were identified as small hydrophobic derivatives of pyrene and nitropyrene, showing significantly brighter emission than CND. We conclude
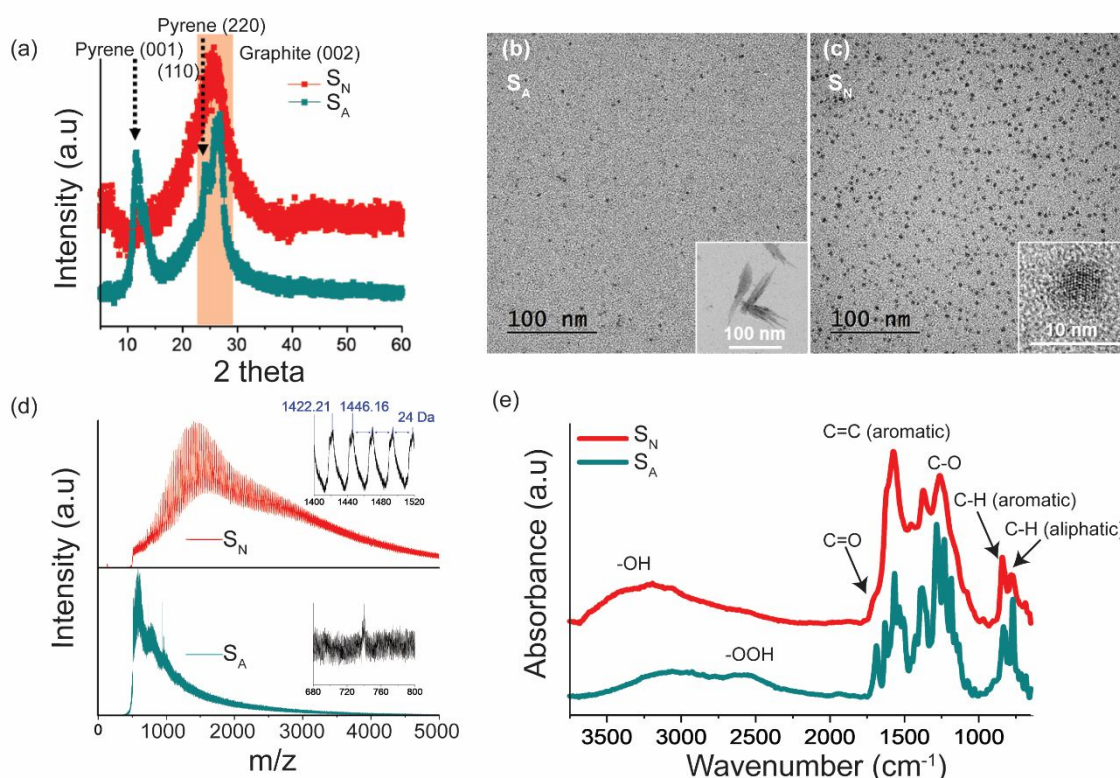


Figure 5. (a) XRD spectra of $S_A$ and $S_N$. TEM images of (b) $S_A$ and (c) $S_N$. Insets in the figures show the high-resolution TEM images of $S_A$ and $S_N$. (d) MALDI-TOF mass spectra of $S_A$ and $S_N$. (e) FT-IR spectra of $S_A$ and $S_N$.

The PLs of $S_A$, $S_N$, and the remaining residue after the washouts were collected to confirm emissive species present in each washout, as shown in Figure S7 (a-c). PL spectrum of $S_A$ (Fig. S7(a)) resembles those of $F_Y$ and $F_G$. The sharp emission in the blue region corresponds to pyrene monomer emission. Clearly the majority of molecular fluorophores are partitioned to $S_A$. This is in a good agreement with the results of MALDI-TOF, TEM and XRD analyses. PL spectrum of the $S_N$ (Fig. S7(b)) appears as the combination of molecular fluorophore and the real CND. Possibly some molecular fluorophore molecules can be partitioned into $S_N$ together with CND into since molecular fluorophores also contains hydroxyl groups. PL spectrum of the washout residue (Fig. S7(c)) is very similar to that of $F_{CND}$ which mainly contains the CND. This suggests that CND with very little or no hydroxyl groups remain in the residue without being extracted into the base solution.

that molecular fluorophores and CND are clearly dissimilar in chemical structure and optical properties. This work sheds a light on the formation of hydrophobic molecular fluorophores in the synthesis of PAH-derived CND, which was rarely reported in the community. It also highlights the need of rigorous separation and purification steps in the synthesis of not only hydrophilic CND but also low-oxygen-content CND.

## Author Contributions

S.W.K., H.-J.S., H.C., B.-S.K., and D.Y.K. participated in conceiving and designing the project. S.W.K., M.S., and H.-J.S. contributed to synthesis and characterization of carbon dots. N.L.K., N.H.K., C.J.H., and B.-S.K. and D.Y.K. contributed to the separation of carbon dots and molecular fluorophores, and their characterizations. F.Y., S.-Y.K., K.Y.H., W.-J.S., and H.C. assisted idea development and data interpretation. All authors have given approval to the final version of

**ARTICLE**

the manuscript.

## Conflicts of interest

There are no conflicts to declare.

## Acknowledgements

## Notes and references

1. Z. Zhang, J. Zhang, N. Chen and L. Qu, *Energy & Environmental Science*, 2012, **5**.
2. X. Du, I. Skachko, A. Barker and E. Y. Andrei, *Nat Nanotechnol*, 2008, **3**, 491-495.
3. Y. Yan, J. Gong, J. Chen, Z. Zeng, W. Huang, K. Pu, J. Liu and P. Chen, *Adv Mater*, 2019, **31**, e1808283.
4. T. Wang, A. Wang, R. Wang, Z. Liu, Y. Sun, G. Shan, Y. Chen and Y. Liu, *Scientific Reports*, 2019, **9**.
5. V. Gupta, N. Chaudhary, R. Srivastava, G. D. Sharma, R. Bhardwaj and S. Chand, *J Am Chem Soc*, 2011, **133**, 9960-9963.
6. W. Kwon, Y. H. Kim, C. L. Lee, M. Lee, H. C. Choi, T. W. Lee and S. W. Rhee, *Nano Lett*, 2014, **14**, 1306-1311.
7. H. B. Yang, Y. Q. Dong, X. Wang, S. Y. Khoo and B. Liu, *ACS Appl Mater Interfaces*, 2014, **6**, 1092-1099.
8. Y. Li, Y. Hu, Y. Zhao, G. Shi, L. Deng, Y. Hou and L. Qu, *Adv Mater*, 2011, **23**, 776-780.
9. Z. Zhu, J. Ma, Z. Wang, C. Mu, Z. Fan, L. Du, Y. Bai, L. Fan, H. Yan, D. L. Phillips and S. Yang, *J Am Chem Soc*, 2014, **136**, 3760-3763.
10. X. T. Zheng, A. Than, A. Ananthanaraya, D. H. Kim and P. Chen, *ACS Nano*, 2013, **7**, 6278-6286.
11. S. Zhu, J. Zhang, C. Qiao, S. Tang, Y. Li, W. Yuan, B. Li, L. Tian, F. Liu, R. Hu, H. Gao, H. Wei, H. Zhang, H. Sun and B. Yang, *Chem Commun (Camb)*, 2011, **47**, 6858-6860.
12. Q. Liu, B. Guo, Z. Rao, B. Zhang and J. R. Gong, *Nano Lett*, 2013, **13**, 2436-2441.
13. Y. Dong, C. Chen, X. Zheng, L. Gao, Z. Cui, H. Yang, C. Guo, Y. Chi and C. M. Li, *Journal of Materials Chemistry*, 2012, **22**.
14. L. Li, G. Wu, G. Yang, J. Peng, J. Zhao and J. J. Zhu, *Nanoscale*, 2013, **5**, 4015-4039.
15. J. Liu, R. Li and B. Yang, *ACS Central Science*, 2020, **6**, 2179-2195.
16. D. Qu and Z. Sun, *Materials Chemistry Frontiers*, 2020, **4**, 400-420.
17. F. Yuan, T. Yuan, L. Sui, Z. Wang, Z. Xi, Y. Li, X. Li, L. Fan, Z. A. Tan, A. Chen, M. Jin and S. Yang, *Nature Communications*, 2018, **9**.
18. W. Kwon, S. Do, J.-H. Kim, M. Seok Jeong and S.-W. Rhee, *Scientific Reports*, 2015, **5**, 12604.
19. F. Yuan, Y.-K. Wang, G. Sharma, Y. Dong, X. Zheng, P. Li, A. Johnston, G. Bappi, J. Z. Fan, H. Kung, B. Chen, M. I. Saidaminov, K. Singh, O. Voznyy, O. M. Bakr, Z.-H. Lu and E. H. Sargent, *Nature Photonics*, 2019, **14**, 171-176.
20. N. Fuyuno, D. Kozawa, Y. Miyauchi, S. Mouri, R. Kitaura, H. Shinohara, T. Yasuda, N. Komatsu and K. Matsuda, *Advanced Optical Materials*, 2014, **2**, 983-989.
21. M. Zhao, F. Yang, Y. Xue, D. Xiao and Y. Guo, *Chemphyschem*, 2014, **15**, 950-957.
22. R. L. Calabro, D.-S. Yang and D. Y. Kim, *ACS Applied Nano Materials*, 2019, **2**, 6948-6959.
23. L. Bao, Z. L. Zhang, Z. Q. Tian, L. Zhang, C. Liu, Y. Lin, B. Qi and D. W. Pang, *Adv Mater*, 2011, **23**, 5801-5806.
24. L. Wang, S.-J. Zhu, H.-Y. Wang, Y.-F. Wang, Y.-W. Hao, J.-H. Zhang, Q.-D. Chen, Y.-L. Zhang, W. Han, B. Yang and H.-B. Sun, *Advanced Optical Materials*, 2013, **1**, 264-271.
25. H. Zheng, Q. Wang, Y. Long, H. Zhang, X. Huang and R. Zhu, *Chem Commun (Camb)*, 2011, **47**, 10650-10652.
26. S. Wang, I. S. Cole, D. Zhao and Q. Li, *Nanoscale*, 2016, **8**, 7449-7458.
27. S. Zhu, J. Shao, Y. Song, X. Zhao, J. Du, L. Wang, H. Wang, K. Zhang, J. Zhang and B. Yang, *Nanoscale*, 2015, **7**, 7927-7933.
28. L. Wang, Y. Wang, T. Xu, H. Liao, C. Yao, Y. Liu, Z. Li, Z. Chen, D. Pan, L. Sun and M. Wu, *Nat Commun*, 2014, **5**, 5357.
29. J. B. Essner, J. A. Kist, L. Polo-Parada and G. A. Baker, *Chemistry of Materials*, 2018, **30**, 1878-1887.
30. V. Hinterberger, C. Damm, P. Haines, D. M. Guldi and W. Peukert, *Nanoscale*, 2019, **11**, 8464-8474.
31. R. Liu, D. Wu, X. Feng and K. Mullen, *J Am Chem Soc*, 2011, **133**, 15221-15223.
32. Y. Song, S. Zhu, S. Zhang, Y. Fu, L. Wang, X. Zhao and B. Yang, *Journal of Materials Chemistry C*, 2015, **3**, 5976-5984.
33. L. Shi, J. H. Yang, H. B. Zeng, Y. M. Chen, S. C. Yang, C. Wu, H. Zeng, O. Yoshihito and Q. Zhang, *Nanoscale*, 2016, **8**, 14374-14378.
34. V. Strauss, H. Wang, S. Delacroix, M. Ledendecker and P. Wessig, *Chemical Science*, 2020, **11**, 8256-8266.
35. N. Dhenadhayalan, K.-C. Lin, R. Suresh and P. Ramamurthy, *The Journal of Physical Chemistry C*, 2016, **120**, 1252-1261.
36. T. Lee, S. Won, Y. Park and W. Kwon, *ACS Applied Nano Materials*, 2021, **4**, 2462-2469.
37. S. Kaplan, *Organic Magnetic Resonance*, 1981, **15**, 197-199.
38. H. S. Rosenkranz, E. C. McCoy, D. R. Sanders, M. Butler, D. K. Kiriazides and R. Mermelstein, *Science*, 1980, **209**, 1039-1043.
39. J. Wu, W. Pisula and K. Mullen, *Chem Rev*, 2007, **107**, 718-747.
40. X. Yang, X. Dou, A. Rouhanipour, L. Zhi, H. J. Rader and K. Mullen, *J Am Chem Soc*, 2008, **130**, 4216-4217.
41. P. G. Ren, D. X. Yan, X. Ji, T. Chen and Z. M. Li, *Nanotechnology*, 2011, **22**, 055705.
42. N. C. Verma, A. Yadav and C. K. Nandi, *Nat Commun*, 2019, **10**, 2391.
43. R. Rajendran, S. Sohila, R. Muralidharan, C. Muthamizhchelvan and S. Ponnusamy, *European Journal of Inorganic Chemistry*, 2014, **2014**, 392-396.
44. M. El Idrissi, S. J. Teat, P. F. Corvini, M. J. Paterson, S. J. Dalgarno and P. Shahgaldian, *Chem Commun (Camb)*, 2017, **53**, 1973-1976.
45. A. Rizzi, P. Cosmina, C. Flego, L. Montanari, R. Seraglia and P. Traldi, *J Mass Spectrom*, 2006, **41**, 1232-1241.
46. L. Becker, T. E. Bunch and L. J. Allamandola, *Nature*, 1999, **400**, 227-228.